Defect Classification for 2D-Material STEM Datasets

Vikas Reddy Paduri[1]*, Nirmal Singh[1], Prabhat Prajapati[1], Mehran Yasir[2], Vinayak Srivastava[3], Karishma Begum[4], Abinava Yeshwanth K.J.[5]

[1]Department of Mechanical and Aerospace Engineering, Oklahoma State University, Stillwater, OK 74078, USA
[2]Department of Physics, Oklahoma State University, Stillwater, OK 74078, USA
[3]Department of Chemical Engineering, Oklahoma State University, Stillwater, OK 74078, USA
[4]Department of Computer Science and Information Technology, Oklahoma State University, Stillwater, OK 74078, USA
[5]Department of Biosystems & Agricultural Engineering, Oklahoma State University, Stillwater, OK 74078, USA
*Correspondence: vpaduri@okstate.edu

Motivation

Two-dimensional Janus transition metal dichalcogenides, such as MoWSSe, exhibit a rich variety of atomic-scale defects, including vacancies, interstitials, and antisite defects, that strongly influence their electronic, optical, and catalytic properties. High-angle annular dark-field (HAADF) STEM imaging provides atomic-resolution contrast that enables direct visualization of these defects. However, manual identification and classification of all defect types across large experimental datasets are impractical and incomplete, as many defects are subtle, rare, or spatially heterogeneous. While domain experts can identify prominent defects by visual inspection, a significant fraction of defects remains difficult to detect consistently. This limitation motivates the need for a machine learning-based defect classification framework that can scale beyond human inspection and enable statistical analysis of defect populations [1].

Methodology

We employed a two-stage hybrid workflow for automated defect identification and classification in HAADF-STEM images of Janus MoWSSe. In Stage 0 (physics-guided pre-processing), atomic column positions and corresponding HAADF intensities were extracted to form unit-cell-level descriptors. Leveraging the strong HAADF Z-contrast under our imaging conditions, these intensity distributions enable interpretable separation of S, Se, Mo, and W atomic species and provide physically meaningful inputs for learning. Building on these descriptors, a CNN-based supervised model performs hierarchical defect classification, where Stage 1 distinguishes perfect from defective unit cells and Stage 2 further assigns defective cells to antisite, vacancy, or interstitial categories. The network was trained on 64×64-pixel patches, and large-area defect mapping was carried out on 512×512 images using sliding-window inference to generate patch-level probability heatmaps; predicted defect regions were subsequently converted into contours and bounding boxes to enable automated localization and quantitative analysis across the full field of view [2].

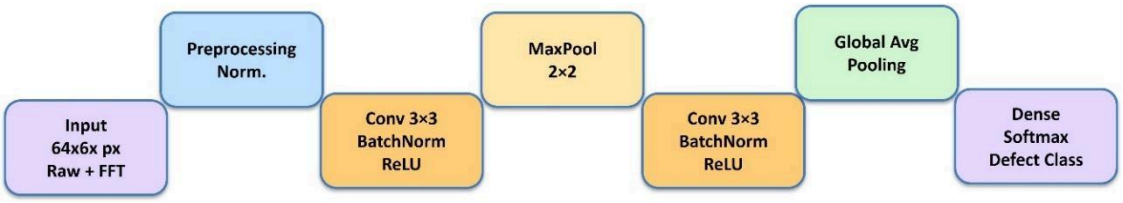

Fig. 1. Model Architecture of the CNN deployed for training on classified data.

Results

Using the proposed workflow, we achieved automated, atomically resolved defect identification and classification in HAADF-STEM images of Janus MoWSSe. The

physics-guided descriptor stage robustly extracted atomic column locations and HAADF intensities, enabling unit-cell-level atom counting and chemically informed labeling. Intensity distributions were sufficiently separable to support consistent assignment of S, Se, Mo, and W columns across broad image regions, remaining stable under experimental noise and moderate local lattice distortion. The supervised classifier used these physics-informed descriptors to distinguish pristine from defective unit cells and to categorize defect subtypes. On unseen test data, the classifier achieved 71 % overall accuracy for Stage 1 (perfect vs defective) and 68% overall accuracy for Stage 2 (antisite vs vacancy vs interstitial). The large-area sliding-window workflow enabled scalable defect mapping, producing probability heatmaps from which contours and bounding boxes were automatically extracted to quantify defect distributions beyond manual, region-limited inspection [3].

Composition and class statistics. Aggregating predictions across the analyzed regions yields the following compositional distribution: W (26.71%), SSe (23.39%), Mo (22.84%), Se_2 (13.36%), and S_2 (11.76%), with vacancy-related classes occurring at low frequency: V_B(Se) = 1.18% and V_B(S) = 0.76%. Here, the reported percentages represent the fraction of classified unit-cell or patch assignments (as defined by the inference aggregation used for Fig. 2). The low vacancy fractions are consistent with sparse missing-atom events relative to dominant lattice configurations, while the presence of mixed/chalcogen-related classes (e.g., SSe, S_2, Se_2) reflects measurable compositional variability captured by the model at scale.

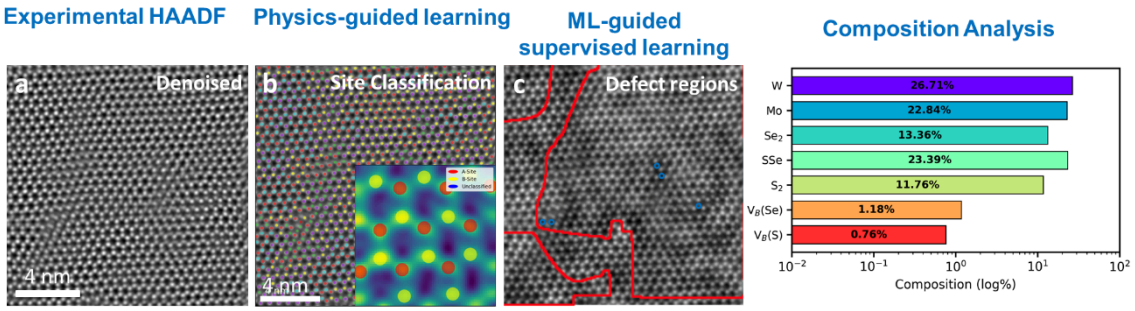

Fig. 2. Defect identification and composition mapping from HAADF-STEM. (a) Representative experimental HAADF image (input; denoised). (b) Physics-guided deep learning output showing atomic-site classification (overlay/inset). (c) ML-guided supervised learning result highlighting defect regions; red contours delineate defects, and inset marks the perfect regions with A and B sites. Right: elemental composition (log scale) extracted and summarized by class.

Conclusion

This work demonstrates a hybrid, physics-guided and supervised-learning workflow for automated defect analysis in HAADF-STEM images of Janus MoWSSe. The approach extracts atomic column positions and Z-contrast intensities to build interpretable descriptors and then performs two-stage defect classification with 71% accuracy for perfect vs defective and 68% accuracy for defect subtype classification on unseen data. Large-area inference via sliding windows enables automated defect localization and lattice-scale statistics, including class-wise composition estimates dominated by W (26.71%), SSe (23.39%), and Mo (22.84%), with low predicted vacancy fractions (≤1.18%). Despite its advantages, the current approach is limited by the availability of labelled training data for rare or weak-contrast defects and by potential sensitivity to variations in imaging conditions such as thickness or drift. Rule-based clustering approaches are insufficient due to their reliance on handcrafted thresholds and poor generalization.

Future work will focus on end-to-end segmentation models, improved class-imbalance handling, uncertainty quantification, and the integration of simulated and multimodal data to enhance robustness and chemical specificity.

Reference

[1] A. Maksov, O. Dyck, K. Wang, K. Xiao, D.B. Geohegan, B.G. Sumpter, R.K. Vasudevan, S. Jesse, S. V. Kalinin, M. Ziatdinov, Deep learning analysis of defect and phase evolution during electron beam-induced transformations in WS_2, NPJ Comput Mater 5 (2019). https://doi.org/10.1038/s41524-019-0152-9.

[2] M. Ziatdinov, O. Dyck, A. Maksov, X. Li, X. Sang, K. Xiao, R.R. Unocic, R. Vasudevan, S. Jesse, S. V. Kalinin, Deep Learning of Atomically Resolved Scanning Transmission Electron Microscopy Images: Chemical Identification and Tracking Local Transformations, ACS Nano 11 (2017) 12742–12752. https://doi.org/10.1021/acsnano.7b07504.

[3] S.H. Yang, W. Choi, B.W. Cho, F.O.T. Agyapong-Fordjour, S. Park, S.J. Yun, H.J. Kim, Y.K. Han, Y.H. Lee, K.K. Kim, Y.M. Kim, Deep Learning-Assisted Quantification of Atomic Dopants and Defects in 2D Materials, Advanced Science 8 (2021). https://doi.org/10.1002/advs.202101099.

[4] Oak Ridge National Laboratory Center for Computational Sciences. (n.d.). *HAADF-STEM dataset for atomic-scale defect analysis* [Data set]. https://doi.ccs.ornl.gov/dataset/78833284-28a4-59da-9790-3624a6f8b9e3.

[5] https://github.com/Karishma-2212/MIC_Hackthon_Team_Nanobots.